



# Rapid and efficient uptake of aqueous lead pollutant using starch-based superabsorbent hydrogel

Chukwunonso O. Aniagor<sup>1</sup> · M. A. Affi<sup>2</sup> · A. Hashem<sup>2</sup>

Received: 13 April 2021 / Revised: 2 June 2021 / Accepted: 28 June 2021 /  
Published online: 7 July 2021

© The Author(s), under exclusive licence to Springer-Verlag GmbH Germany, part of Springer Nature 2021

## Abstract

The need for a viable and sustainable environment has triggered the increased preference for eco-friendly agro-based biosorbents to synthetic ones. In this study, a superabsorbent hydrogel ('*c-hydrogel*') synthesized from a renewable agro-based precursor via polyacrylonitrile (PAN) graft copolymerization and subsequent hydrolysis was utilized for aqueous lead [Pb(II)] uptake. The chemical structure (using Fourier transform infrared spectroscopy, FTIR equipment), surface morphology (using scanning electron microscopy, SEM equipment) and the physicochemical properties of the synthesized '*c-hydrogel*' were investigated. Similarly, the effect of some process variables on the biosorbents' adsorption capacity, as well as the process equilibrium and kinetics modelling, was also undertaken in the study. The isotherm data were best fitted to the Langmuir and Temkin model, with a maximum adsorption capacity of 264.37 mg/g and fast kinetics of 40 min at pH 5.0. Conversely, the kinetic data were well fitted to the pseudo-first-order model. The '*c-hydrogel*' showed a high water absorbency of 550 g water/g '*c-hydrogel*' and demonstrated effectiveness, as a renewable and eco-friendly biosorbent for the aqueous lead ion [Pb (II)] removal.

**Keywords** Hydrogel · Adsorption · Lead ion · Kinetics · Isotherm

## Introduction

Heavy metal pollutants pose a major environmental sustainability challenge [1–3]. Due to their relative non-degradability, these highly toxic contaminants readily accumulate within living cells and as such cause serious long-term health

---

✉ Chukwunonso O. Aniagor  
co.aniagor@unizik.edu.ng

✉ A. Hashem  
alhashem2000@yahoo.com

<sup>1</sup> Department of Chemical Engineering, Nnamdi Azikiwe University, P.M.B. 5025, Awka, Nigeria

<sup>2</sup> Textile Research Division, National Research Centre, Dokki, Cairo, Egypt

damages [1, 4, 5]. Lead ion is one of the most commonly identified aqueous contaminants in the battery, paint, dye and pigment industrial waste streams [1, 6]. However, due to non-stringent waste disposal regulations and improper industrial effluent disposal habit, some of these lead ions make their way into the food chain (either in drinking waters or contaminated seafood). Based on literature reports, the risk of lead ion pollution is enormous, as they can readily metabolize into an invasive poison, with a strong enzymatic inhibitory effect [7]. Also, prolonged exposure to lead contamination mainly through the ingestion/consumption of lead-contaminated substances can result in various disease such as renal failure, mental ineptitude and anaemia [1, 5, 8]. Since their permissible contamination limit is set at  $0.05 \text{ mg L}^{-1}$  [9], lead ion uptake using an efficient technique is paramount.

Considering the aforementioned negative consequences of lead pollution, coupled with their relative non-degradability, the need for their effective sequestration from the aqueous environment is further justified. Consequently, various techniques like ion exchange, membrane filtration, chemical precipitation, electrodeposition have been applied for aqueous Pb(II) uptake [10–12]. Meanwhile, the large scale application of these remedial techniques has shown several disadvantages which include poor thermostability and reusability [13], exorbitant operational cost [11] and generation of a huge volume of post-treatment sludge [14]. The biosorption technique using low-cost biosorbent precursor is currently explored as an efficient alternative for treating heavy metal-laden wastewater. The preference for the biosorption approach is related to its operational flexibility, process efficiency, efficient regeneration of spent adsorbent, etc. [15].

The usefulness of natural polymers-based biosorbents in heavy metal sorption either in its raw or modified form has been reported [4, 16–21]. However, the existence of structural crystallinity and high amylose content reduced the sorption capacity of the raw polymers by limiting the cationic species' access to the active sites of these polymers [22]. To forestall such limitation, researches into the chemical modification/functionalization (via improvement of the available functional groups) of these native carbohydrate polymers are currently in progress [1]. Polymer sorbent functionalization is often achieved through different chemical techniques like copolymer grafting, hydrolysis, etc. [23]. The graft copolymerization process is used to introduce relevant metal-binding sites such as carboxyl, amino group, etc., as well as significantly modify the starch/polymer network [22, 24]. Abd El-Ghany et al. [25] and Abd El-Ghany et al. [26] synthesized novel hydrogel adsorbents by grafting of corn starch and 4-acrylamidobenzoic acid (4ABA). During the hydrogel synthesis, diallyldimethylammonium chloride and ammonium persulfate (APS)/sodium bisulfite were used as the cross-linker and redox initiator, respectively. By varying the concentration of the crosslinker, thermally stable hydrogels of high swelling capacity were obtained in the studies.

Therefore, the study aims at the synthesis of copolymerized starch-based hydrogel (*c-hydrogel*) via a two-stage process involving grafting of polyacrylonitrile to the native starch and further hydrolysis of the copolymerized starch to hydrogels. The lead ion adsorption properties of the synthesized '*c-hydrogel*' adsorbent were evaluated under the effect of certain process variable via batch mode. Furthermore, physicochemical,

morphological and structural characteristics, as well as the equilibrium and kinetic modelling behaviour of the '*c-hydrogel*', was elucidated in the study.

## Materials and methods

### Materials

Corn starch was obtained from the Egyptian Starch and Glucose Manufacturing Company, Cairo, Egypt. All other laboratory grade reagents utilized in this work including polyacrylonitrile, ammonium cerium (IV) nitrate (CAN), lead acetate, etc., were supplied by Merck, Germany.

### Methods

#### Graft procedure

The procedure followed in this study for the polyacrylonitrile-starch grafting was according to an earlier procedure reported by Abdel-Halim [16], with slight modifications. The procedure involves the gelatination of a 2.0 g of dried corn starch in a suitable (enough to form a gel) volume of water contained in a 100 mL Erlenmeyer flask. The mixture was heated to and maintained at 85 °C for 30 min using a thermostatic water-bath. Afterwards, 50 mL of polyacrylonitrile and 10 mL of a binary mixture of freshly prepared ammonium cerium (IV) nitrate and 1 N HNO<sub>3</sub> (comprising 1:2 ratio, respectively) were introduced into the flask containing the already cooled (30–33 °C) gelatinized starch. The set-up was left to stand for 1 h at ambient temperature (30 ± 3°C) and continuous stirring (150 rpm).

The reaction by-products (homopolymers) were further eliminated via the precipitation of the starch copolymer in N, N-dimethylformamide (DMF). The resultant precipitates (homopolymer-free graft-starch) were consequently obtained, washed with deionized water and then oven-dried at 50 °C to constant dry weight. Following the micro-Kjeldahl method [27], the % nitrogen content of the graft-starch was estimated, while the % graft yield was evaluated from Eq. (1) [21, 28].

$$\% \text{Graft yield} = \frac{\left[ \frac{(N(\%)*53)}{14} * 100 \right]}{\left[ \frac{100 - (N(\%)*53)}{14} \right]} \quad (1)$$

NB: 53 and 14 are the molecular weight (g/mol) of polyacrylonitrile and nitrogen (N), respectively.

#### Hydrogel synthesis

1.0 g of the grafted starch composite was treated with 10 mL of 0.7 N NaOH in a loosely stoppered (to permit ammonia evolution) flask. The mixture was mechanically

stirred using a thermostatic magnetic stirrer (at 150 rpm and 95 °C) until the completion of the saponification (indicated by a solution colour change from deep red to light yellow). Afterwards, the hydrolyzed gel was dispersed in a predetermined volume of methanol (coupled with stirring for 5 min) and subsequently charged into an excess volume of ethanol. The precipitate was washed with acidified ethanol until neutrality, filtered off and oven-dried (60 °C, 3 h) to obtain the superabsorbent hydrogel (*'c-hydrogel'*).

### Hydrogel swelling capacity measurement

In the procedure, 1.0 g of the *'c-hydrogel'* was impregnated in distilled water (100 mL) at ambient temperature ( $30 \pm 3^\circ\text{C}$ ) and left to absorb water until its saturation point. The fully swollen *'c-hydrogel'* was recovered as filtrate, drained and reweighed. The water absorption capacity of the *'c-hydrogel'* was evaluated from Eq. (2) [16, 28].

$$\text{Swelling capacity} \left( \frac{\text{g}}{\text{g}} \right) = \frac{M_2 - M_1}{M_1} \quad (2)$$

where  $M_1$  and  $M_2$  are the masses of swollen *'c-hydrogel'* and dry *'c-hydrogel'*.

### Adsorption experiments

By dissolving an appropriate amount of lead acetate in deionized water, the stock solution ( $1 \text{ g L}^{-1}$ ) was obtained. Meanwhile, the working lead ion concentrations were further achieved from the serial dilution (using deionized water) of the stock solution.

During the adsorption experiment, a predetermined amount of *'c-hydrogel'* was charged into the adsorbate solution (100 mL) contained in a 250 mL conical flask. The mixture was stirred mechanically using a magnetic stirrer (Stuart, Model UC151/120 V/60) at 150 rpm and 30 °C. At a specified interval, test samples were withdrawn from the mixture, filtered through Whatman No. 41 filter paper and the remaining lead ion concentration was measured using atomic absorption spectrophotometer (AAS, ZA3000, HITACHI, Japan). By varying the solution pH using either 0.1 M  $\text{HNO}_3$  or 0.1 M  $\text{NaOH}$  as appropriate, the effect of pH studies was investigated in the pH range of 2.0–5.0. Similarly, the effect of time (0–60 min) and adsorbent dosage (0.3–4.0 g/L) was also investigated.

The associated adsorption parameters such as the % uptake efficiency (RE %) and the amount of lead ion adsorbed at equilibrium ( $q_e$ ) are calculated from Eqs. (3)–(4), respectively.

$$\text{RE} (\%) = \frac{C_o - C_e}{C_o} \cdot 100\% \quad (3)$$

$$q_e = \frac{(C_o - C_e) V}{W} \quad (4)$$

where  $C_o$ =Initial lead ion concentration ( $\text{mg L}^{-1}$ ),  $C_e$ =lead ion concentration at equilibrium ( $\text{mg L}^{-1}$ ),  $W$ =Mass of '*c-hydrogel*' used (g),  $V$ =volume of adsorbate solution used (L).

## Adsorption modelling

### Kinetics models

The kinetic evaluation for the study was conducted using the pseudo-first-order, PFO [29] and pseudo-second-order, PSO [30] model at varying initial adsorbate concentrations. The mathematical expression of the PFO and PSO models is, respectively, presented in Eqs. (5) and (6).

$$q_t = q_e [1 - \exp(-k_1 t)] \quad (5)$$

$$q_t = \frac{k_2 * q_e^2 * t}{(1 + k_2 * t)} \quad (6)$$

NB: PFO and PSO rate constants are denoted by  $k_1$  (1/min) and  $k_2$  (g/(mg min)), respectively.

### Isotherm models

Four classical and commonly applied isotherm models, namely the Langmuir [31], Freundlich [32], Temkin [33] and Dubinin–Radushkevich [34] models, were investigated for modelling the equilibrium data. The mathematical expression, as well as other analogue equations associated with the respective isotherm models, is presented in Table 1.

### Error function models

In this study, the kinetic and isotherm model parametric evaluations were achieved via the nonlinear regression of the respective experimental kinetic and equilibrium data using the solver function of the Microsoft Excel, 2016 model. Considering the inadequacy of the coefficient of determination alone for describing nonlinearly regressed data, six error function models were consequently adopted. The error models include the average relative error, ARE [35], average percentage error, APE [36], the sum of squared error, SSE [37], hybrid fraction error, HYBRID [38], Marquardt's Percent Standard Deviation, MPSD [35] and nonlinear chi-square test,  $\chi^2$  [39]. The mathematical expressions of these error model are shown in Table 2. Notably, the error models generated a given error value for each of the isotherm and kinetic models. Due to obvious inconsistency in the obtained error values and the need to perform holistic analyses, the error values were subsequently normalized following the guide provided by Hashem et al. [40] and Menkiti et al. [41] to obtain

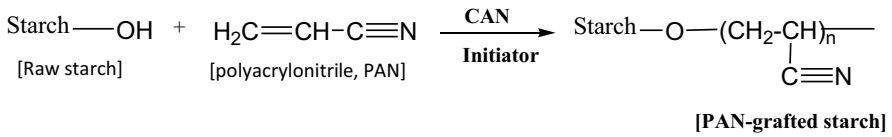
**Table 1** The applied isotherm model equations

Model name	Model equation
Langmuir	$q_e = \frac{q_m k_L C_e}{1 + k_L C_e}$ $R_L = \frac{1}{1 + K_L C_o}$
Freundlich	$q_e = K_F (C_e)^{\frac{1}{n_F}}$
Tempkin	$q_e = \frac{RT}{b_T} \ln (K_T C_e)$
D–R*	$q_e = q_D * \exp \left\{ -\beta_D \left[ RT \left( 1 + \frac{1}{C_e} \right) \right]^2 \right\}$ $E = \frac{1}{\sqrt{2\beta_{DR}}}$

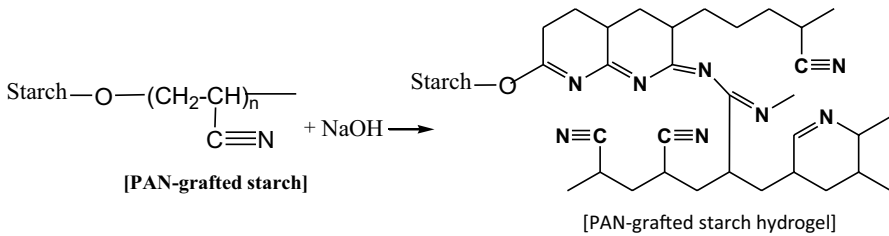
NB:  $q_e$  (mg/g) and  $C_e$  (mg/L) are the adsorption capacity per unit mass of adsorbent and the adsorbates' equilibrium concentration, respectively. The  $q_m$  (mg/g) denotes the monolayer adsorption capacity, while  $k_L$  (L/mg) and  $R_L$  are the Langmuir constants.  $K_F$  (mg/g) and  $n_F$  are Freundlich parameters that denote Freundlich the adsorption capacity and adsorption intensity, respectively. The  $K_T$  and  $b_T$  are Temkin constants, while  $\beta_D$  is the D–R model constant  
D–R\* Dubinin–Radushkevich

**Table 2** Mathematical expression of the different error function models

Error function	Equation
Average relative error (ARE)	$ARE = \sum_{i=1}^n \left  \frac{(q_e)_{exp.} - (q_e)_{calc.}}{(q_e)_{exp.}} \right $
Average percentage error (APE)	$APE\% = \frac{\sum_{i=1}^n \left  \left[ \frac{(q_e)_{exp.} - (q_e)_{calc.}}{(q_e)_{exp.}} \right] \right }{N} \times 100$
Sum squares error (ERRSQ/SSE)	$ERRSQ = \sum_{i=1}^n \left[ (q_e)_{calc.} - (q_e)_{exp.} \right]^2$
Hybrid fraction error function (Hybrid)	$Hybrid = \frac{100}{n-p} \sum_{i=1}^n \left[ \frac{\left( \frac{(q_e)_{exp.} - (q_e)_{calc.}}{(q_e)_{exp.}} \right)^2}{(q_e)_{exp.}} \right]$
Marquardt's percent standard deviation (MPSD)	$MPSD = \left( \frac{100}{n-p} \sqrt{\frac{1}{\sum_{i=1}^n \left[ \frac{\left( \frac{(q_e)_{exp.} - (q_e)_{calc.}}{(q_e)_{exp.}} \right)^2}{(q_e)_{exp.}} \right]}} \right)$
Nonlinear chi-square test ( $\chi^2$ )	$\chi^2 = \sum \frac{(q_e, exp - q_e, theoretical)^2}{q_e, theoretical}$
Coefficient of determination ( $R^2$ )	$R^2 = \frac{\sum_{i=1}^n (q_{e, calc} - \overline{q_{e, exp}})^2}{\sum_{i=1}^n (q_{e, calc} - \overline{q_{e, exp}})^2 + \sum_{i=1}^n (q_{e, calc} - q_{e, exp})^2}$



**Scheme 1** Schematic representation for the synthesis of PAN-grafted starch



**Scheme 2** Schematic representation for the conversion of the grafted starch to hydrogel

the sum of normalized error (SNE) values. Meanwhile, the isotherm and kinetic model that depicts the lowest SNE value is thus considered the best fit.

## Results and discussion

### Mechanism of hydrogel synthesis

The reaction stages (polyacrylonitrile grafting and hydrogel formation) involved during the synthesis of the biosorbent (*c-hydrogel*) are represented stoichiometrically in Schemes 1 and 2. The polymerization reaction between the starch hydroxyl groups and the polyacrylonitrile (PAN) compound in the presence of ammonium cerium (IV) nitrate, (CAN) initiator, afforded the PAN grafted starch as shown in Scheme 1. By subjecting the PAN grafted starch to further saponification reaction with sodium hydroxide, the desired hydrogel biosorbent (*c-hydrogel*) is obtained as illustrated in Scheme 2.

### Biosorbent characterization

#### Surface morphology studies

The SEM equipment [TESCAN CE VEGA 3 SBU (117–0195- Czech Republic)] operated at 1000× magnification was used to obtain the surface morphologies of the raw starch, grafted starch and *c-hydrogel*. The resulting SEM images as presented in Fig. 1a–c show the resemblance of a heterogenous woollen matrix assemblage, with fibrous interconnections. Upon further visual comparison, no significant differences were observed between Fig. 1a, b. This is because the polyacrylonitrile grafting simply introduced nitrogen-based functional groups which could only be

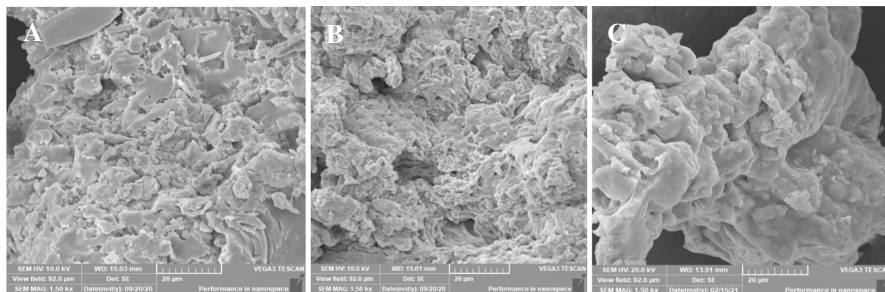


**Fig. 1** SEM images for **a** gelatinized maize starch **b** grafted starch and **c** 'c-hydrogel'

elucidated by surface chemistry analyses. Meanwhile, better surface aggregated patches of superior particle agglomeration, surface roughness and porosity were observed in the hydrolysed grafted starch, 'c-hydrogel' (Fig. 1c). These 'c-hydrogel' characteristics of beneficial for cation binding.

### Surface chemistry studies

The available surface functional groups of the biosorbent sample and the precursors were obtained using FTIR equipment (FT-IR spectrometer 4100 JASCO – JAPAN). Following the KBr disc technique, the spectra were recorded in the range of  $400\text{--}4000\text{ cm}^{-1}$  (scanning speed:  $2\text{ mm/sec}$ , resolution:  $4\text{ cm}^{-1}$ ). Figure 2 (FTIR spectra for raw starch, grafted starch and 'c-hydrogel') is characterized with some common and identical peak at wavenumbers  $3290\text{ cm}^{-1}$  (H-bonded OH stretch),  $2927\text{ cm}^{-1}$  (C–H stretch) and  $1010\text{ cm}^{-1}$  (C–O stretch) [42]. The amide C=O stretch domicile at  $1543\text{ cm}^{-1}$  was very pronounced in the c-hydrogel spectra when compared to that of the raw and grafted starch. Similarly, the C–H stretch of the grafted starch was suppressed sequel to the saponification reaction. Consequently, several

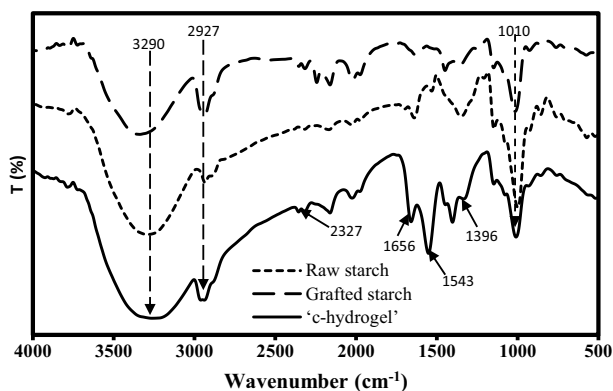


**Fig. 2** The FTIR spectra of raw starch, grafted starch and 'c-hydrogel'



**Table 3** The ‘*c-hydrogel*’ physicochemical characterization result

N% in grafted starch composite	N% in hydrolyzed grafted starch (Hydrogel)	Water uptake (g/g)
10.3	3.0	550

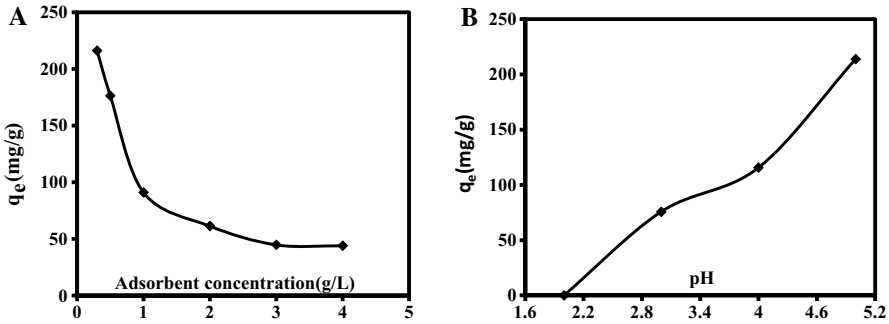


**Fig. 3** The effect of **a** adsorbent concentration and **b** solution pH on adsorption capacity

nitrogen-based functional groups introduced during polyacrylonitrile grafting were identified on the ‘*c-hydrogel*’ spectra at  $1396\text{ cm}^{-1}$  (CN stretch) and  $1656\text{ cm}^{-1}$  (NH bend of primary amine).

**Physicochemical analyses result**

The extent of grafting expressed as % nitrogen content and the water absorption capacity of the biosorbent are shown in Table 3. The % nitrogen content of the ‘*c-hydrogel*’ is about 3 times less than that of the PAN grafted starch. This result is very much as expected since most of the cyano groups of the grafted starch were converted to amide and carboxylate groups during hydrogel formation. However, these carboxylate groups were not so pronounced in the FTIR analyses result as they were subsequently eliminated from the saponification precipitates.

Furthermore, the water absorption capacity of the synthesized ‘*c-hydrogel*’ is recorded as 550 g water/g ‘*c-hydrogel*’ (Table 3). This water absorption value is reasonably high and according to Abdel-Halim [16], such high water absorbency could have resulted from the structural alteration (such as molecule disorientation, free volume magnification, etc.) associated with the PAN copolymer grafting.

**Effect of the process variable**

The relationship between the adsorbent dosage and the adsorption capacity is very useful in the study of adsorption systems as they relate to the number of adsorption sites [43]. A plot of the aforementioned relationship as presented in Fig. 3. The plot depicted an inverse relationship between both factors (adsorption capacity and adsorbent dosage). An increase in the adsorbent dosage from 0.3 to 4.0 g/L

resulted in about an 80% reduction in the adsorption capacity. Hence, for every 1.0 g/L increase in adsorbent dosage, there is about a 10% reduction in the adsorption capacity until no more substantive adsorption capacity was recorded (beyond 4.0 g/L adsorbent dosage). The above observation is explained thus, at the initial low adsorbent dosage (0.3 g/L), there is a high affinity between the adsorbate molecules and the available active sites [44]. However, as the amount of adsorbent increased, the adsorption capacity dropped (despite the supposed active sites increment), due to possible active sites clogging, overcrowding and interference [45].

A proper study and understanding of the pH effect on a given metal ion adsorption system is key to establishing the nature and degree of interaction between the adsorbent and adsorbate [46]. According to Fig. 3b, a consistent increase in adsorbate solution pH from pH 2.0 to pH 5.0 favoured the adsorption capacity and raised it from 0 mg/g (at pH 2.0) to 213.8 mg/g (at pH 5.0). This observation is due to significant protonation of the '*c-hydrogel*' active sites at lower pH ranges, thus resulting in ionic competition between the adsorbates and the hydrogen ion ( $H^+$ ). Preliminary studies showed a reduction in adsorption capacity as the adsorbate solution pH was increased beyond pH 5.0 due to precipitation of the lead molecules as hydroxides. Therefore, the optimum adsorbate solution pH condition was established at pH 5.0.

## Equilibrium studies

Equilibrium studies help in predicting the maximum adsorption capacity, uptake process design and biosorbent optimization for large scale applications [47, 48]. The present study evaluated the fitting ability of four (4) classical 2-parameter isotherm models (namely Langmuir, Freundlich, Temkin and Dubinin–Radushkevich models) to the experimental equilibrium data. The isotherm plot generated for the study is presented in Fig. 4. The plot showed an ordered curve line of initial rapid adsorption which further equilibrated towards the equilibrium concentration ( $C_e$ ) axis at a higher concentration range. This isotherm shape is typical of an L-type isotherm based on the Giles classification system [49] and specifies progressive '*c-hydrogel*'

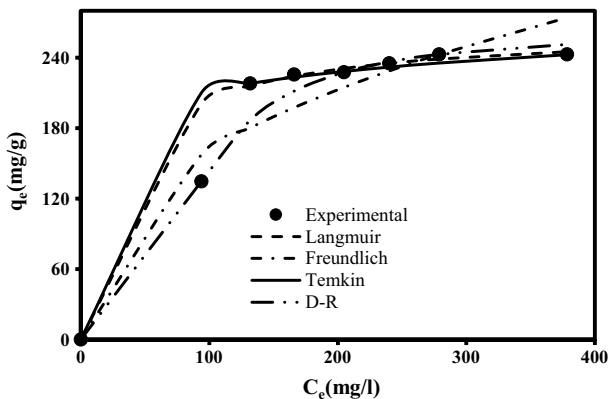


Fig. 4 Isotherm model plots

**Table 4** Isotherm model parameters

Langmuir	Freundlich	Temkin	D–R*
$q_{\max} = 264.37$	$n_F = 2.51$	$A_T = 89.68$	$q_D = 261.92$
$K_L = 8.88$	$K_F = 25.87$	$b_T = 108.30$	$\beta_D = 9.3E-04$
$R_L = 0.033$	$R^2 = 0.987$	$R^2 = 0.982$	$R^2 = 0.996$
$R^2 = 0.986$			

*D–R\** Dubinin–Radushkevich

**Table 5** Error values for isotherm modelling

Langmuir	Freundlich	Temkin	D–R*
ARE = 0.548	ARE = 0.681	ARE = 0.618	ARE = 0.248
APE = 7.835	APE = 9.730	APE = 8.829	APE = 3.538
EABS = 79.501	EABS = 139.555	EABS = 89.061	EABS = 55.404
ERRSQ = 4402.719	ERRSQ = 3939.494	ERRSQ = 5776.996	ERRSQ = 1259.337
Hybrid = 32.571	Hybrid = 18.916	Hybrid = 42.679	Hybrid = 5.708
MPSD = 0.241	MPSD = 0.095	MPSD = 0.316	MPSD = 0.026
$X^2 = 21.909$	$X^2 = 19.826$	$X^2 = 27.448$	$X^2 = 6.515$
<b>SNE = 1.032</b>	<b>SNE = 1.048</b>	<b>SNE = 1.029</b>	<b>SNE = 1.057</b>

*D–R\** Dubinin–Radushkevich

sites saturation during biosorption. Furthermore, L-type isotherm is analogous to monolayer adsorption, with significant adsorbate–biosorbent interaction and negligible solvent-adsorbate ionic competition [50].

Tables 4 and 5, respectively, present the nonlinearly regressed isotherm parameters and the corresponding sum of normalized error values for the respective models. The result shows that the Langmuir ( $R^2 = 0.986$  &  $SNE = 1.032$ ) and Temkin ( $R^2 = 0.982$  &  $SNE = 1.029$ ) model provided the best fit to the experimental equilibrium data despite the higher  $R^2$  values depicted by the Freundlich ( $R^2 = 0.987$ ) and D–R ( $R^2 = 0.996$ ) models. This decision on the best fit model was reached on basis of the sum of normalized error (SNE) values, as the Freundlich and D–R models depicted relatively larger SNE values. The Langmuir maximum adsorption capacity was recorded as 264.37 mg/g, while its  $R_L$  value indicates favourable adsorption, as well as confirms the biosorbent effectiveness. Similarly, the large positive Temkin constant ( $b_T$ ) value is synonymous with the exothermic adsorption process. The emergence of the Langmuir and Temkin model as the top best fit models suggests the predominance of the homogeneous monolayer chemisorption process [51]. This finding is also in line with the earlier proposed L-type isotherm classification.

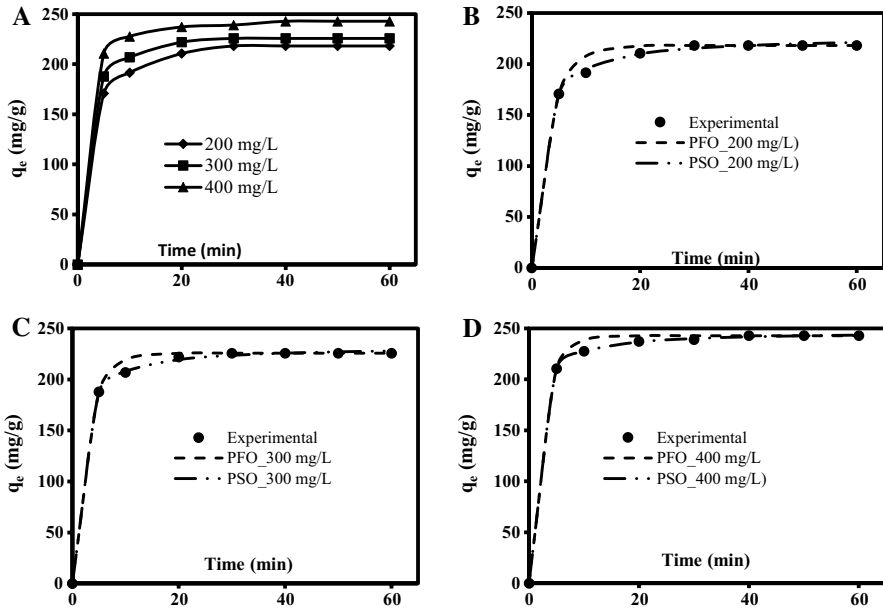


**Fig. 5** Plots of the **a** effect of contact time **b** kinetic model plot for 200 mg/L system **c** kinetic model plot for 300 mg/L system **d** kinetic model plot for 400 mg/L system

## Kinetics studies

The effect of contact time on the amount of Pb (II) adsorbed at varying concentrations is presented in Fig. 5a. Judging from the plot, an initial fast adsorption rate was experienced within the first 5 min of biosorbent-adsorbate contact, while attaining about 87% (for 400 mg/L system), 83% (for 300 mg/L system) and 78% (for 200 mg/L system) of the total and optimum adsorbed amount at the respective initial concentrations. Such finding is an indication of a high affinity between the ‘*c-hydrogel*’ and the Pb (II) ion. The uptake rate subsequently equilibrated at 40 min at all initial concentrations, with optimum adsorption amounts of 242.77, 225.70 and 218.14 mg/g for 400, 300 and 200 mg/L adsorption systems. The observed increment in the amount of lead ion adsorbed as the initial adsorbate concentration increased is attributed to an increase in the chemical potential and concentration instilled driving force at higher initial adsorbate concentration [52].

For the modelling of experimental kinetic data, two classical and fundamental models (namely, pseudo-first-order, PFO and pseudo-second-order, PSO) were applied at varying initial adsorbate concentrations. The generated kinetic plot, the corresponding SNE values and the nonlinearly regressed parameters are presented in Fig. 5b–d, Tables 6 and 7, respectively. According to the data presented in the Tables, both the PFO and PSO model depicted some reasonably high  $R^2$  values ( $>0.9$ ) at all initial adsorbate concentrations. Meanwhile, the second-order adsorption rate constant ( $k_2$ ) was quite lower than the first-order rate constant ( $k_1$ ), thus implying faster adsorption concerning the PSO. Despite all these important

**Table 6** Error values for kinetic modelling

200 mg/L		300 mg/L		400 mg/L	
PFO	PSO	PFO	PSO	PFO	PSO
ARE=0.12	ARE=0.06	ARE=0.08	ARE=0.0412	ARE=0.087	ARE=0.014
APE=1.70	APE=0.79	APE=1.10	APE=0.589	APE=1.249	APE=0.206
EABS=23.37	EABS=11.62	EABS=16.21	EABS=9.17	EABS=20.30	EABS=3.45
ERRSQ=314.28	ERRSQ=31.43	ERRSQ=171.59	ERRSQ=18.55	ERRSQ=164.23	ERRSQ=2.89
Hybrid=1.617	Hybrid=0.151	Hybrid=0.825	Hybrid=0.083	Hybrid=0.713	Hybrid=0.012
MPSD=8E-03	MPSD=7E-04	MPSD=4E-03	MPSD=4E-04	MPSD=3E-03	MPSD=5E-05
$\chi^2=1.501$	$\chi^2=0.150$	$\chi^2=0.781$	$\chi^2=0.083$	$\chi^2=0.685$	$\chi^2=0.012$
SNE=1.090	SNE=1.406	SNE=1.111	SNE=1.537	SNE=1.140	SNE=1.907

**Table 7** Kinetic model parameters

	Pseudo-first order	Pseudo-second order
200 mg/L		
	$q_e = 218.11$	$q_e = 227.13$
	$k_1 = 0.31$	$k_2 = 2.6E-03$
	$R^2 = 0.998$	$R^2 = 0.999$
300 mg/L		
	$q_e = 225.70$	$q_e = 232.41$
	$k_1 = 0.36$	$k_2 = 3.6E-03$
	$R^2 = 0.999$	$R^2 = 0.999$
400 mg/L		
	$q_e = 242.76$	$q_e = 246.96$
	$k_1 = 0.40$	$k_2 = 4.6E-03$
	$R^2 = 0.999$	$R^2 = 0.999$

NB:  $q_{e, \text{exp}} = 218.14$  mg/g (for 200 mg/L), 225.73 mg/g (for 300 mg/L) and 242.77 mg/g (for 400 mg/L)

parameters depicted by PSO, it is considered unfit for modelling the experimental kinetic data, since its SNE value is larger than that of PFO at all initial adsorbate concentration. Also, the PSO calculated adsorption capacity as shown in Table 7 varied widely from the experimentally derived adsorption capacity. Thus, the PFO with the lowest SNE values at all initial adsorbate concentrations is selected as the model of best fit. The first-order adsorption rate ( $k_1$ ) and calculated adsorption capacity ( $q_{e, \text{cal}}$ ) ranged from 0.31 to 0.40 (1/min) and 218.11 to 242.76 mg/g and were found to consistently increase with an increase in initial adsorbate concentration. Similarly, the strong numerical correlation between the experimentally derived ( $q_{e, \text{exp}}$ ) and PFO calculated ( $q_{e, \text{cal}}$ ) adsorption capacity is a further confirmation of the superior fitting of the PFO model.

## Conclusion

A low-cost starch-based hydrogel ('*c-hydrogel*') was successfully synthesized and subsequently applied for lead ion adsorption. Due to its structural modification and reduced carboxylate group repulsion, the '*c-hydrogel*' achieved a pure water swelling capacity of 550 g water/g '*c-hydrogel*'. The % nitrogen content of the '*c-hydrogel*' was about 3 times less than that of its direct precursor (PAN grafted starch) due to the conversion of some of its cyano groups into amide and carboxylate groups. The experimental equilibrium and kinetic data were modelled accordingly. The Temkin model emerged as the isotherm model of best fit, while the pseudo-first-order model was recorded as the kinetic model of best fit. During the effect of process variable investigations, it was observed that for every 1.0 g/L increase in adsorbent dosage, there is about a 10% reduction in the adsorption capacity until no more substantive adsorption capacity was recorded (beyond 4.0 g/L adsorbent dosage). Similarly, a consistent increase in adsorbate solution pH from pH 2.0 to pH 5.0 favoured the adsorption capacity and raised it from 0 (at pH 2.0) to 213.8 mg/g (at pH 5.0). The study has therefore demonstrated the potential application of '*c-hydrogel*' as a renewable and eco-friendly biosorbent for lead ion removal from wastewater.

## Declarations

**Conflict of interest** The authors declare that there is no known conflict of interest regarding this work.

## References

1. Chakraborty R, Asthana A, Singh AK, Jain B, Susan ABH (2020) Adsorption of heavy metal ions by various low-cost adsorbents: a review. *Int J Environ Anal Chem.* <https://doi.org/10.1080/03067319.2020.1722811>
2. Aniagor CO, Menkiti MC (2020) Relational description of an adsorption system based on isotherm, adsorption density, adsorption potential, hopping number and surface coverage. *Sigma* 38(3):1073–1098
3. Hashem A, Abdel-Halim E, El-Tahlawy KF, Hebeish A (2005) Enhancement of the adsorption of Co (II) and Ni (II) ions onto peanut hulls through esterification using citric acid. *Adsorpt Sci Technol* 23(5):367–380
4. Hashem A, Aniagor C, Taha G, Fikry M (2021) Utilization of low-cost sugarcane waste for the adsorption of aqueous Pb(II): kinetics and isotherm studies. *Curr Res Green Sustain Chem.* <https://doi.org/10.1016/j.crgsc.2021.100056>
5. Li Y-H, Wang S, Wei J, Zhang X, Xu C, Luan Z, Wu D, Wei B (2002) Lead adsorption on carbon nanotubes. *Chem Phys Lett* 357(3–4):263–266
6. Hashem A, Badawy SM (2015) *Sesbania sesban* L. biomass as a novel adsorbent for removal of Pb (II) ions from aqueous solution: non-linear and error analysis. *Green Process Syn* 4(3):179–190
7. Denizli A, Büyüktuncel E, Tuncel A, Bektas S, Genç Ö (2000) Batch removal of lead ions from aquatic solutions by polyethyleneglycol-methacrylate gel beads carrying cibacron blue F3GA. *Environ Technol* 21(6):609–614
8. Hashem A, Fletcher A, Younis H, Mauof H, Abou-Okeil A (2020) Adsorption of Pb (II) ions from contaminated water by 1, 2, 3, 4-butanetetracarboxylic acid-modified microcrystalline cellulose: Isotherms, kinetics, and thermodynamic studies. *Int J Biol Macromol* 164:3193–3203

9. Mahmoud AM, Ibrahim FA, Shaban SA, Youssef NA (2015) Adsorption of heavy metal ion from aqueous solution by nickel oxide nano catalyst prepared by different methods. *Egypt J Pet* 24(1):27–35
10. Duan C, Ma T, Wang J, Zhou Y (2020) Removal of heavy metals from aqueous solution using carbon-based adsorbents: a review. *J Water Process Eng* 37:101339
11. Foong CY, Wirzal MDH, Bustam MA (2020) A review on nanofibers membrane with amino-based ionic liquid for heavy metal removal. *J Mol Liq* 297:111793
12. Zhao Z, Xiong Y, Cheng X, Hou X, Yang Y, Tian Y, You J, Xu L (2020) Adsorptive removal of trace thallium (I) from wastewater: a review and new perspectives. *J Hazard Mater* 393:122378
13. Hosseini S, Alibakhshi H, Jashni E, Parviziyan F, Shen J, Taheri M, Ebrahimi M, Rafiei N (2020) A novel layer-by-layer heterogeneous cation exchange membrane for heavy metal ions removal from water. *J Hazard Mater* 381:120884
14. Wu H, Wang W, Huang Y, Han G, Yang S, Su S, Sana H, Peng W, Cao Y, Liu J (2019) Comprehensive evaluation on a prospective precipitation-flotation process for metal-ions removal from wastewater simulants. *J Hazard Mater* 371:592–602
15. Awual MR, Alharthi NH, Hasan MM, Karim MR, Islam A, Znad H, Hossain MA, Halim ME, Rahman MM, Khaleque MA (2017) Inorganic-organic based novel nano-conjugate material for effective cobalt (II) ions capturing from wastewater. *Chem Eng J* 324:130–139
16. Abdel-Halim ES (2013) Preparation of starch/poly(N, N-Diethylaminoethyl methacrylate) hydrogel and its use in dye removal from aqueous solutions. *React Funct Polym* 73(11):1531–1536
17. Hashem A, Abdel-Halim E, Maaouf H, Ramadan M, Abo-Okeil A (2007) Treatment of sawdust with polyamine for wastewater treatment. *Energ Educ Sci Technol* 19:45–58
18. Hashem A (2006) Amidoximated sunflower stalks (ASFS) as a new adsorbent for removal of Cu (II) from aqueous solution. *Polym-Plast Technol Eng* 45(1):35–42
19. Božić D, Gorgievski M, Stanković V, Štrbac N, Šerbula S, Petrović N (2013) Adsorption of heavy metal ions by beech sawdust—kinetics, mechanism and equilibrium of the process. *Ecol Eng* 58:202–206
20. Mohammed RR (2012) Removal of heavy metals from waste water using black teawaste. *Arab J Sci Eng* 37(6):1505–1520
21. Hashem A, Fletcher A, El-Sakhawy M, Mohamed LA, Farag S (2020) Aminated hydroxymoyl camelthorn residues as a novel adsorbent for extracting Hg (II) from contaminated water: studies of isotherm, kinetics, and mechanism. *J Polym Environ* 28(9):2498–2510
22. Abdel-Halim E, Al-Deyab SS (2014) Preparation of poly (acrylic acid)/starch hydrogel and its application for cadmium ion removal from aqueous solutions. *React Funct Polym* 75:1–8
23. Abdel-Halim E, Abou-Okeil A, Hashem A (2006) Adsorption of Cr (VI) oxyanions onto modified wood pulp. *Polym-Plast Technol Eng* 45(1):71–76
24. Zhou Y, Fu S, Zhang L, Zhan H, Levit MV (2014) Use of carboxylated cellulose nanofibrils-filled magnetic chitosan hydrogel beads as adsorbents for Pb (II). *Carbohydr Polym* 101:75–82
25. Abd El-Ghany NA, Mahmoud ZM (2020) Synthesis, characterization and swelling behavior of high-performance antimicrobial amphoteric hydrogels from corn starch. *Polym Bull.* <https://doi.org/10.1007/s00289-020-03417-8>
26. Abd El-Ghany NA, Aziz MSA, Abdel-Aziz MM, Mahmoud Z (2019) Antimicrobial and swelling behaviors of novel biodegradable corn starch grafted/poly (4-acrylamidobenzoic acid) copolymers. *Int J Biol Macromol* 134:912–920
27. Kjeldahl J (1883) Neue methode zur bestimmung des stickstoffs in organischen körpern. *Z Anal Chem* 22(1):366–382
28. Hashem A, Afifi M, El-Alfy E, Hebeish A (2005) Synthesis, characterization and saponification of poly (AN)-starch composites and properties of their hydrogels. *Am J Appl Sci* 2(3):614–621
29. Anagor C, Menkiti M (2019) Synthesis, modification and use of lignified bamboo isolate for the renovation of crystal violet dye effluent. *Appl Water Sci* 9(4):77
30. Ho Y-S, McKay G (1999) Pseudo-second order model for sorption processes. *Process Biochem* 34(5):451–465
31. Vijayaraghavan K, Padmesh T, Palanivelu K, Velan M (2006) Biosorption of nickel (II) ions onto *Sargassum wightii*: application of two-parameter and three-parameter isotherm models. *J Hazard Mater* 133(1–3):304–308
32. Adamson AW, Gast AP (1967) *Physical chemistry of surfaces*, vol 150. Interscience publishers, New York

33. Temkin M (1940) Kinetics of ammonia synthesis on promoted iron catalysts. *Acta physiochim URSS* 12:327–356
34. Radushkevich M (1947) The equation of the characteristic curve of the activated charcoal USSR. *Phys Chem Sect* 55:331
35. Marquardt DW (1963) An algorithm for least-squares estimation of nonlinear parameters. *J Soc Ind Appl Math* 11(2):431–441
36. Khair U, Fahmi H, Al Hakim S, Rahim R (2017) Forecasting error calculation with mean absolute deviation and mean absolute percentage error. *J Phys Conf Ser* 930:012002
37. Ng J, Cheung W, McKay G (2002) Equilibrium studies of the sorption of Cu (II) ions onto chitosan. *J Colloid Interface Sci* 255(1):64–74
38. Kapoor A, Yang R (1989) Correlation of equilibrium adsorption data of condensable vapours on porous adsorbents. *Gas Sep Purif* 3(4):187–192
39. Rivas F, Beltrán F, Gimeno O, Frades J, Carvalho F (2006) Adsorption of landfill leachates onto activated carbon: equilibrium and kinetics. *J Hazard Mater* 131(1–3):170–178
40. Hashem A, Aniagor C, Hussein D, Farag S (2021) Application of novel butane-1, 4-dioic acid-functionalized cellulosic biosorbent for aqueous cobalt ion sequestration. *Cellulose* 28(6):3599–3615
41. Menkiti M, Aniagor C (2018) Parametric studies on descriptive isotherms for the uptake of crystal violet dye from aqueous solution onto lignin-rich adsorbent. *Arab J Sci Eng* 43(5):2375–2392
42. Nandiyanto ABD, Oktiani R, Ragadhita R (2019) How to read and interpret FTIR spectroscopy of organic material. *Indonesian J Sci Technol* 4(1):97–118
43. Aniagor C, Abdel-Halim E, Hashem A (2021) Evaluation of the aqueous Fe (II) ion sorption capacity of functionalized microcrystalline cellulose. *J Environ Chem Eng*. <https://doi.org/10.1016/j.jece.2021.105703>;p.105703
44. Hashem A, Aniagor CO, Nasr M, Abou-Okeil A (2021) Efficacy of treated sodium alginate and activated carbon fibre for Pb(II) adsorption. *Int J Biol Macromol*. <https://doi.org/10.1016/j.ijbiomac.2021.02.067>;p.1-16
45. Hashem A, Abou-Okeil A, Fikry M, Aly A, Aniagor CO (2021) Isotherm and kinetics parametric studies for aqueous Hg(II) uptake onto n-[2-(methylamino)ethyl]ethane-1,2-diaminated acrylic fibre. *Arab J Sci Eng*. <https://doi.org/10.1007/s13369-021-05416-x>
46. Asuquo E, Martin A, Nzerem P, Siperstein F, Fan X (2017) Adsorption of Cd (II) and Pb (II) ions from aqueous solutions using mesoporous activated carbon adsorbent: equilibrium, kinetics and characterisation studies. *J Environ Chem Eng* 5(1):679–698
47. Oba SN, Ighalo JO, Aniagor CO, Igwegbe CA (2021) Removal of ibuprofen from aqueous media by adsorption: a comprehensive review. *Sci Total Environ*. <https://doi.org/10.1016/j.scitotenv.2021.146608>;p.146608
48. Igwegbe CA, Oba SN, Aniagor CO, Adeniyi AG, Ighalo JO (2020) Adsorption of ciprofloxacin from water: a comprehensive review. *J Ind Eng Chem* 93:57–77
49. Giles CH, Smith D, Huitson A (1974) A general treatment and classification of the solute adsorption isotherm. I. Theoretical. *J Colloid Interface Sci* 47(3):755–765
50. Limousin G, Gaudet J-P, Charlet L, Szenknect S, Barthes V, Krmissa M (2007) Sorption isotherms: a review on physical bases, modeling and measurement. *Appl Geochem* 22(2):249–275
51. Aniagor CO, Igwegbe CA, Ighalo JO, Oba SN (2021) Adsorption of doxycycline from aqueous media: a review. *J Mol Liq*. <https://doi.org/10.1016/j.molliq.2021.116124>;p.116124
52. Elliott J, Ward C (1997) Chemical potential of adsorbed molecules from a quantum statistical formulation. *Langmuir* 13(5):951–960

**Publisher's Note** Springer Nature remains neutral with regard to jurisdictional claims in published maps and institutional affiliations.